Available online at www.sciencedirect.com

SciVerse ScienceDirect

Procedia Computer Science 18 (2013) 2512 – 2520

Procedia Computer Science

International Conference on Computational Science, ICCS 2013

Simulating mobile dendrites in a flow

Dmitry Medvedev[*,a,b], Fathollah Varnik[a], Ingo Steinbach[a]

[a]*Interdisciplinary Centre for Advanced Materials Simulation (ICAMS), Ruhr University Bochum, Stiepeler Str. 129, 44780, Bochum, Germany*
[b]*Lavrentyev Institute of Hydrodynamics, Siberian Branch of Russian Academy of Sciences, Lavrentyev prosp. 15, 630090, Novosibirsk, Russia*

Abstract

We propose a scheme for simulation of the solute-driven dendritic solidification which accounts for the flows of liquid and motion of growing dendrites. The scheme is based on the multiphase-field method for calculating the solidification and the lattice Boltzmann method to simulate the fluid flows. Motion and rotation of solid grains is possible.

Key words: dendritic solidification; flow; lattice Boltzmann equation

1. Introduction

Dendritic solidification is a phenomenon with immense technical and theoretical importance. Its technical importance clearly stems from the fact that the overwhelming majority of all metallic workpieces have once in their lifetime undergone solidification with a dendritic structure. In fact: this transformation allows to encapsulate the heavy segregation, which is inevitably connected to alloy solidification, between the arms of the dendrite on the micrometer scale and thus limits macrosegregation to a considerable extend. Without this feature, no large scale casting could be produced with a controllable alloy composition throughout the casting. The formation of dendritic arms itself is an intrinsic feature of alloy solidification, where the growing interface is morphologically unstable [1] and the dendritic structure evolves from self-organization. The basic theories of dendritic solidification [2, 3, 4, 5, 6] deal with purely diffusive conditions. Under terrestrial conditions it is, however, evident that there is buoyancy driven flow which affects the growth conditions of the dendrites significantly [7]. Recently, a scaling theory was developed by one of the authors [8] which predicts a decreasing or increasing primary spacing dependent on the orientation of flow with respect to the vector of gravity: there is a complex interaction of flow with dendritic growth since the dendritic network will limit the flow through friction at the solid structures on the one hand. On the other hand, flow increases transport of solute and thereby influences the growth of dendrites. These mutual interactions can be self-accelerating or self-restricting dependent on the direction of flow. The reader is referred to [8] for more details. In that work the solid dendrites were assumed to be rigidly fixed, e.g., being attached to the bottom of the mold in a directional solidification furnace. An even more challenging task is the case of equiaxed dendrites freely floating in a melt. There will be different situations, e.g., upward buoyancy of solutal plumes and downward sedimentation of dendrites due to the

[*]Corresponding author
Email address: dmitry.medvedev@rub.de (Dmitry Medvedev)

Selection and peer review under responsibility of the organizers of the 2013 International Conference on Computational Science
doi:10.1016/j.procs.2013.05.431

density difference between solid and liquid. Also the dendrites will rotate, as described in [9]. To be able to investigate this complex behavior more closely, we aim to develop a phase-field model of solutal solidification combined with a robust fluid flow solver. The lattice-Boltzmann (LB) method is presently a well-established tool to simulate fluid flows, especially flows in complex geometries [10, 11, 12].

The first combinations of the Phase field approach with the lattice Boltzmann method to include hydrodynamic flow effects on the solidification phenomena goes back to the studies of Fabritiis and coworkers [13] and Miller and coworkers [14, 15, 16]. Guided by one of the well known lattice Boltzmann pioneers, Sauro Succi, these authors investigated dendritic growth in a pure melt in externally imposed flows. Results obtained by these simulations showed the great potential of the new combined method in accurately dealing with the mutual interplay of an evolving complex solidification pattern on the one hand and the flow around this pattern on the other hand, the latter influencing back the solidification process via the transport of heat which is created at the solidification front. These promising investigations motivated additional studies of the topic by independent research groups, who extended the range of the applications of the method to binary alloys and other flow situations [17, 18, 19].

In all these studies, however, the solid phase was assumed to be immobile. The challenge to be overcome is to include rigid-body motion and rotation in the model. In the present work, we address this issue firstly in a 2-dimensional approximation. Generalization of the proposed approach to three dimensions is straight-forward and is left to future work.

2. Numerical model

2.1. Phase field method

The phase-field method has now become a method of choice to simulate the dendritic solidification. Its main advantage is the absence of the need of front tracking, together with the possibility of keeping good accuracy at moderate computational cost, if a thin-interface approach such as the one discussed by Karma and Rappel [20, 21] is employed. The method has been used for the simulation of thermal-driven solidification from a pure melt as well as the solute-driven solidification of alloys [22].

In the present work, we use the multi-phase field model described in [23, 24]. The free energy functional consists of several terms corresponding, e.g., to the interfacial f^{GB} and chemical f^{CH} free energy.

$$F = \int_{\Omega} \left(f^{GB} + f^{CH} + \ldots \right) dV. \tag{1}$$

Other terms like elastic, magnetic and electric energy may be added depending on the problem.

In this work, we use only one phase field ϕ which represents the fraction of the solid phase in a node. The fraction of the liquid phase is $\phi_l = 1 - \phi$. The interfacial (or grain-boundary) free energy density is given by

$$f^{GB} = \frac{4\sigma(\mathbf{n})}{\eta} \left\{ |\nabla\phi|^2 + \frac{\pi^2}{\eta^2}\phi(1-\phi) \right\}, \tag{2}$$

where $\sigma(\mathbf{n})$ is the anisotropic surface energy, η is the width of the interface between two phases, $\mathbf{n} = \nabla\phi/|\nabla\phi|$ is the local normal to the interface.

The chemical part of the free energy is built from bulk free energies of the individual phases

$$f^{CH} = h(\phi) f_s(C_s) + h(1-\phi) f_l(C_l) + \mu(C - (\phi_s C_s + \phi_l C_l)). \tag{3}$$

Here, C is the overall concentration of the solute, and $f_s(C_s)$ and $f_l(C_l)$ are the chemical bulk free energy densities of the solid and the liquid pahses which depend on the concentrations C_s and C_l in the solid and liquid phases, respectively, μ is the generalized chemical potential or diffusion potential of solute introduced as a Lagrange multiplier to conserve the solute mass balance between the phases, $C = \phi_s C_s + \phi_l C_l$. The function h is

$$h(\phi) = \frac{1}{4}\left[(2\phi - 1)\sqrt{\phi(1-\phi)} + \frac{1}{2}\arcsin(2\phi - 1) \right]. \tag{4}$$

Using the free energy functional (1), the kinetic equations for the phase field and concentration variables are constructed

$$\dot{\phi} = -M_\phi \frac{\delta F}{\delta \phi}, \tag{5}$$

$$\dot{C} = M_C \nabla \frac{\delta F}{\delta C}, \tag{6}$$

with the interface mobility M_ϕ and the chemical mobility matrix M_c.

The kinetic equation for the phase field (5) can be explicitly rewritten as

$$\dot{\phi} + \mathbf{u}_s \cdot \nabla \phi = M_{eff} \left\{ \sigma(\mathbf{n}) \left[\nabla^2 \phi + \frac{\pi^2}{\eta^2} \left(\phi - \frac{1}{2} \right) \right] + \frac{\pi}{\eta} \sqrt{\phi(1-\phi)} \Delta G \right\}. \tag{7}$$

The second term in the left hand side represents the advection of phase field with the velocity of solid, $\mathbf{u}_s$.

The evolution equation for the concentration of solute becomes

$$\dot{C} + \mathbf{u}_l \cdot \nabla \left((1-\phi) C_l \right) + \mathbf{u}_s \cdot \nabla \left(\phi C_s \right) = \nabla \cdot \left(D_l (1-\phi) \nabla C_l \right) + \nabla \cdot \mathbf{j}_{at}. \tag{8}$$

with the diffusion coefficient in the liquid D_l and no diffusion in the solid (one-sided model is used). Here, the advection fluxes with the velocities $\mathbf{u}_l$ in the liquid phase and $\mathbf{u}_s$ in the solid phase are introduced. Last term in the right-hand side is the antitrapping current which is necessary to eliminate the effect of numerical solute trapping due to diffusiveness of the interface. It is expressed as

$$\mathbf{j}_{at} = \frac{\eta}{\pi} \sqrt{\phi(1-\phi)} \left(C_l - C_s \right) \dot{\phi} \frac{\nabla \phi}{|\nabla \phi|}. \tag{9}$$

We use a linear phase diagram with the constant partition coefficient $k = c_s/c_l$. The driving force ΔG in the Eq. (5) is $\Delta G = \Delta S (T_m - T - m_l c_l)$ where ΔS is the entropy difference between phases, T_m is the melting temperature of a pure substance, and m_l is the liquidus slope. In order to suppress the kinetic undercooling, we set the effective mobility M_{eff} in the Eq. (5) to

$$M_{eff} = \frac{8 D_l}{\Delta S \eta m_l (c_l - c_s)}.$$

2.2. The lattice Boltzmann method

To obtain the fluid velocity, the Navier-Stokes equation should be solved

$$\frac{\partial}{\partial t} \left((1-\phi) \mathbf{u}_l \right) + \nabla \cdot \left((1-\phi) \mathbf{u}_l \mathbf{u}_l \right) = -\frac{(1-\phi)}{\rho_0} \nabla P + \nabla \cdot \left[\nu \nabla \left((1-\phi) \mathbf{u}_l \right) \right] - h^* \frac{\nu \phi^2 \phi_l (\mathbf{u}_l - \mathbf{u}_s)}{\eta^2} \tag{10}$$

with the liquid density ρ_0 and the kinematic viscosity ν. The last term in the right-hand side is the friction between liquid and the solid which guarantees a no-slip condition in the thin-interface limit. The numerical coefficient $h^* = 145.8$ was fitted from a calculation of Poiseille flow in a channel with diffuse walls, similar to the approach described in [25].

We do not solve the Navier-Stokes equation directly. Instead, we use the lattice Boltzmann method (LBM) [10, 11, 26] to simulate the fluid flow. LBM uses one-particle distribution functions f_k defined at the nodes of a regular spatial lattice as main variables. Different labels k correspond to different velocities $\mathbf{c}_k$ from a fixed finite set. In the two-dimensional nine velocity (D2Q9) model used here, these velocities are $\mathbf{c}_0 = (0,0)$, $\mathbf{c}_k = (\cos((k-1)\pi/2), \sin((k-1)\pi/2))\Delta x/\Delta t$ for $k = 1 \ldots 4$, and $\mathbf{c}_k = \sqrt{2}(\cos((k-1/2)\pi/2), \sin((k-1/2)\pi/2))\Delta x/\Delta t$ for $k = 5 \ldots 8$. Here, Δx is the grid spacing, equal for both the x and y directions, Δt is the time step. The effect of making the velocities proportional to $\Delta x/\Delta t$ is that nonzero velocities lead to nearest neighbour and next-nearest neighbour sites of the square lattice in one time-step, i.e., only lattice point positions appear in the dynamics, no interpolations are necessary.

The evolution equation for f_k is

$$f_k(t + \Delta t, \mathbf{x} + \mathbf{c}_k \Delta t) = f_k(t, \mathbf{x}) + \frac{f_k^{eq} - f_k}{\tau} \Delta t. \tag{11}$$

Distribution functions are advected (first term on the r.h.s.) and undergo a relaxation to equilibrium values f_k^{eq} which are, as usual, taken to be expansions of Maxwellians up to second order in the fluid velocity $\mathbf{U}$

$$f_k^{eq} = \rho w_k \left(1 + \frac{\mathbf{c}_k \cdot \mathbf{U}}{a_s^2} + \frac{(\mathbf{c}_k \cdot \mathbf{U})^2}{2a_s^4} - \frac{U^2}{2a_s^2}\right), \tag{12}$$

with a_s having the physical meaning of an isothermal sound velocity. The local fluid density is given by $\rho = \sum\limits_k f_k = \sum\limits_k f_k^{eq}$, the flow velocity is $\mathbf{U} = \sum\limits_k f_k \mathbf{c}_k / \rho$, and the weight coefficients are $w_0 = 4/9, w_{1-4} = 1/9, w_{5-8} = 1/36$. This form of the equilibrium distribution functions ensures mass and momentum conservation and provides the correct form of the momentum flux tensor [11, 27].

Performing a Chapman-Enskog expansion, one can derive from (11) the continuity and Navier-Stokes equations [11], with kinematic viscosity $\nu = a_s^2(\tau - \Delta t/2)$. For the present D2Q9 lattice, the isothermal sound velocity is $a_s = \Delta x/\sqrt{3}\Delta t$. For small flow velocities the fluid is almost incompressible (effects of compressibility are proportional to U^2/a_s^2).

As mentioned above, the interaction between the growing pattern and the fluid flow was simulated as proposed in [25, 28]. An additional dissipative force was introduced in partially filled regions

$$\mathbf{F}_d = -h^*(1-\phi)\rho_0 \nu \frac{\phi^2}{\eta^2}(\mathbf{U} - \mathbf{u}_s).$$

This provides the correct velocity boundary conditions at the diffuse interface (see [25, 28]), i.e., the sharp-interface limit of the velocity boundary conditions of Eq. (10) is correctly reproduced.

The action of forces on a liquid was simulated by the exact difference method of [29]. The term $\Delta f_k = f_k^{eq}(\rho, \mathbf{U} + \Delta\mathbf{U}) - f_k^{eq}(\rho, \mathbf{U})$ is added to the r.h.s. of eq. (11), where $\Delta\mathbf{U} = \mathbf{F}\Delta t/\rho$ is the velocity change due to the action of force $\mathbf{F}$ at time step Δt. This form of the change of distribution functions is exact in the case where the distribution is equilibrium before the action of the force (then after the action the distribution remains equilibrium), hence the name of the method. In the case of a non-equilibrium initial state, this method is accurate to second order in $\Delta\mathbf{U}$. It is simple enough and valid for arbitrary lattices and any dimension of space. The physical flow velocity $\mathbf{u}_l$ is defined as

$$\mathbf{u}_l = \mathbf{U} + \Delta\mathbf{U}/2$$

which coinsides with $\mathbf{U}$ when the force is zero.

The total force acting on the grain is

$$\mathbf{F} = -\sum \mathbf{F}_d. \tag{13}$$

The total torque acting on the grain is

$$\mathbf{N} = -\sum (\mathbf{r} - \mathbf{R}_{cm}) \times \mathbf{F}_d, \tag{14}$$

where $\mathbf{R}_{cm} = \sum \mathbf{r}\phi(\mathbf{r}) / \sum \phi(\mathbf{r})$ is the radius-vector of the center of mass of the grain.

Equations of motion of the grain are

$$\dot{\mathbf{R}}_{cm} = \mathbf{U}_{cm}, \ \dot{\mathbf{U}}_{cm} = \mathbf{F}/V \tag{15}$$

for the translational motion and

$$\dot{\alpha} = \omega, \ \dot{\omega} = \mathbf{N}/I \tag{16}$$

for the rotation. Here, $\mathbf{U}_{cm}$ is the center of mass velocity, α is the rotation angle, ω is the angular velocity, $V = \rho \sum \phi(\mathbf{r})$ is the total mass of the grain, and $I = \sum \phi(\mathbf{r})(\mathbf{r} - \mathbf{R}_{cm})^2$ is the moment of inertia. Local velocity of solid is given by

$$\mathbf{u}_s = \mathbf{U}_{cm} + \omega \times (\mathbf{r} - \mathbf{R}_{cm}).$$

Equations (5) and (8) are discretized on a square lattice with a grid spacing Δx and solved by a direct Euler method with a time step Δt. Advection of the phase field ϕ is calculated by the Lax-Wendroff method or by the third-order CIP scheme [30, 31], advection of the concentration by the upwind method.

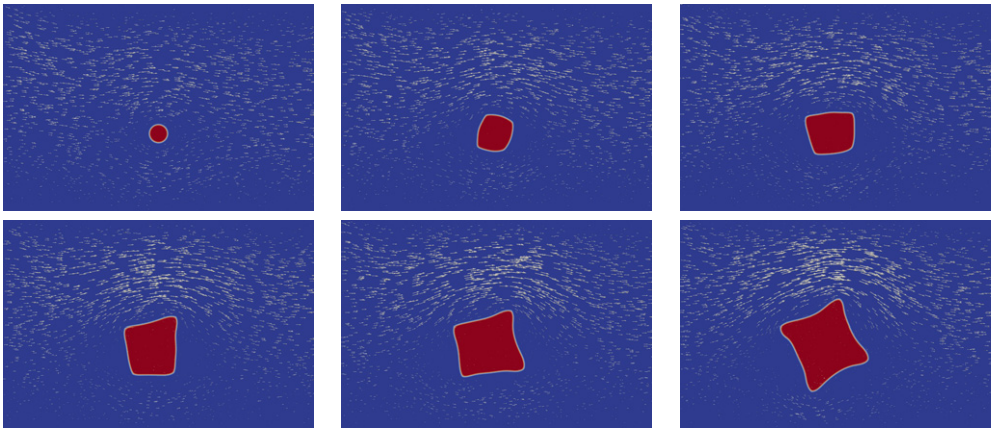

Figure 1: Rotation of a grain in a channel flow. Time is (left to right, top to bottom) t = 0 s, 2 s, 4 s, 6 s, 8 s, 10 s

3. Simulation results

We simulated the growth of a single solid grain from a liquid in different flow environments. The material data for the Al-Cu alloy are given in Table 1. Preferential growth along principal axes was ensured setting the anisotropy of the interface energy in the form

$$\sigma = \sigma_0 \left(1 - 3\epsilon + 4\epsilon \left(n_x^4 + n_y^4 + n_z^4\right)\right)$$

where $\boldsymbol{n}$ is the local normal vector to the interface calculated relative to the rotation angle α. The strength of the anisotropy was $\epsilon = 0.7$. In all simulations, the grid spacing was $\Delta x = 10^{-6}$ m, the time step $\Delta t = 10^{-5}$ s. The temperature was fixed at $T = 922.2$ K which means an undercooling of 1.0 K with respect to the initial composition.

3.1. Rotating grain in a channel flow

A single grain with initial radius $20\Delta x$ was put in a channel of the length $L_x = 400 \cdot 10^{-6}$ m and the width $L_y = 300 \cdot 10^{-6}$ m. The initial position was $x_0 = 0.6L_x$, $y_0 = 0.4L_y$. A flow of liquid with the initial solute concentration $C_0 = 4$ % Cu was set at the boundary $x = 0$ and the conditions $\partial \mathbf{u}_l/\partial x = 0$, $\partial \phi/\partial x = 0$, $\partial C/\partial x = 0$ were imposed at the boundary $x = L_x$. At the sides, the no-flux conditions were imposed for the solute concentration and the phase field, and the no-slip condition for the flow velocity. The incoming profile of the flow velocity was parabolic

$$u_x = 4u_0 y(L_y - y)/L_y^2$$

corresponding to the Poiseille flow. The grain was allowed to rotate but the center of mass position was kept fixed.

Simulation results are shown in Fig. 1. The grain begins to rotate clockwise because of the off-center placement, and a vortex is formed below the grain. The upwind tip grows faster since the flow brings fresh material into its vicinity.

Table 1: Material data used for simulation of dendritic growth in $Al_{96}Cu_4$

Melting point Al	T_m	933.6 K
Liquidus slope	m_l	2.6 K/%
Partition coefficient	k	0.14
Liquid diffusivity	D_l	$3 \cdot 10^{-9}$
Interface energy	σ_0	0.24 J/m^2
Interface energy anisotropy	ϵ	0.7
Density variation	$\frac{1}{\rho}\frac{\partial \rho}{\partial c}$	0.01 1/%
Kinematic viscosity	ν	$5.7 \cdot 10^{-5}$ m^2/s

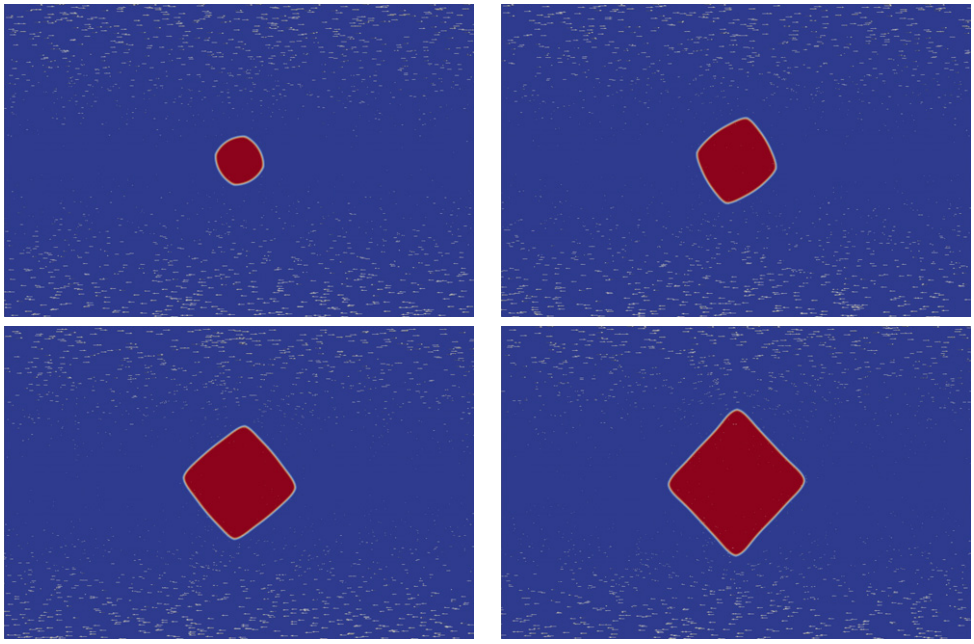

Figure 2: Grain in a shear flow. Time is (left to right, top to bottom) t = 1 s, 4 s, 7 s, 10 s

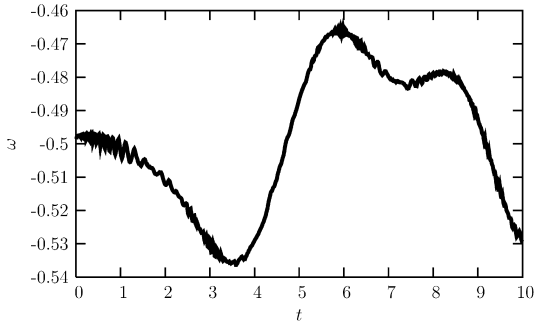

Figure 3: Grain in a shear flow. Time dependence of the grain angular velocity

3.2. Grain in a shear flow

A single grain with initial radius $20\Delta x$ was put in a channel of the length $L_x = 400 \cdot 10^{-6}$ m and the width $L_y = 300 \cdot 10^{-6}$ m. The initial position was $x_0 = L_x/2$, $y_0 = L_y/2$. A constant flow velocity was imposed at the walls $u_x = 2 \cdot 10^{-4}$ m/s at $y = 0$ and $u_x = -2 \cdot 10^{-4}$ m/s at $y = L_y$. The boundary conditions at $x = 0$, $x = L_x$ for the flow were periodic, and a fresh material ($C = C_0$) was fed in. The grain was allowed to move and to rotate.

Simulation results are shown in Fig. 2. The grain rotates clockwise under the action of the flow. The time dependence of the angular velocity is shown in Fig. 3. After the initial transient, the angular velocity increases, then decreases because of the increased drag acting on the branches. This rotation effectively mixes the solute concentration near the interface, and the growth is rather symmetric.

3.3. Moving grain in a channel flow

A single grain with initial radius $20\Delta x$ was put in a channel of the length $L_x = 400 \cdot 10^{-6}$ m and the width $L_y = 300 \cdot 10^{-6}$ m. The initial position was $x_0 = 0.6L_x$, $y_0 = 0.4L_y$. A flow of liquid with the initial solute concentration $C_0 = 4$ % Cu was set at the boundary $x = 0$ and the conditions $\partial \mathbf{u}_l/\partial x = 0$, $\partial \phi/\partial x = 0$, $\partial C/\partial x = 0$ were

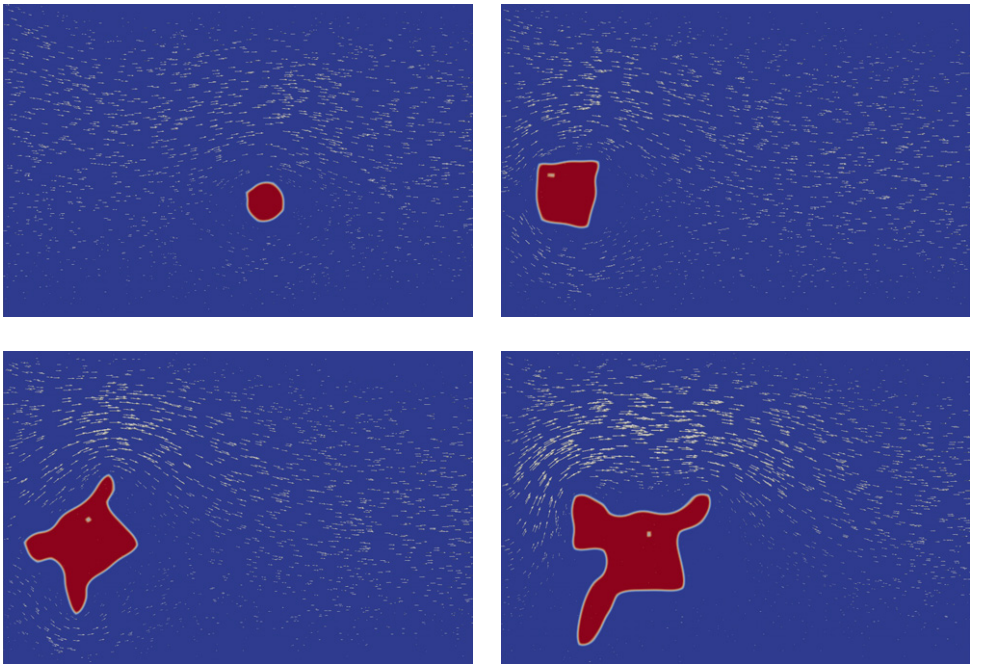

Figure 4: Moving grain in a channel flow. Time is (left to right, top to bottom) $t = 0.5$ s, 1 s, 1.5 s

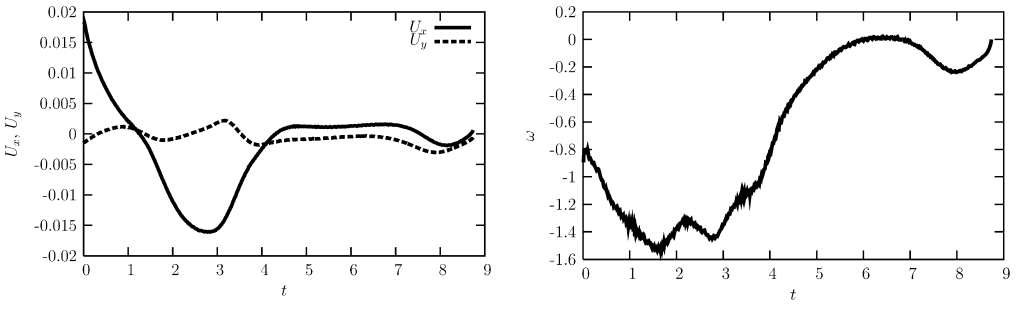

Figure 5: Moving grain in a channel flow. Time dependence of the grain velocity (left) and angular velocity (right)

imposed at the boundary $x = L_x$. At the sides, the no-flux conditions were imposed for the solute concentration and the phase field, and the no-slip condition for the flow velocity. The input profile of the flow velocity was parabolic

$$u_x = 4u_0 y(L_y - y)/L_y^2, \; u_y = 0$$

corresponding to the Poiseille flow. A gravity force acted on the grain with an effective acceleration

$$g_x = -0.12\,\mathrm{m/s^2}, \; g_y = 0.$$

The grain was allowed to move and to rotate.

Simulation results are shown in Fig. 4. The grain moves in the direction of gravity and rotates. Again, the upwind tip grows faster. Time dependence of the center of mass velocity and the angular velocity is shown in Fig. 5. When the size of the grain increases, the drag force also increases, and the grain stops and then starts to move with the flow. The angular velocity also first increases, then decreases and changes sign.

4. Conclusions

In conclusion, we propose a mesoscopic scheme to simulate dendritic solidification with motion and rotation of grains. The scheme is based on the phase-field and the lattice Boltzmann method.

We simulated the growth of a single rotating grain in a duct flow, the growth of a single moving and rotating grain in a shear flow and in a duct flow with the action of gravity. In the first two cases, the grain rotates, in the last case the rotation is less pronounced. In all cases, the upwind tip grows faster. This model shall be extended to 3-dimensions and applied in large scale simulations in future work.

Acknowledgment

The authors would like to acknowledge financial support from ThyssenKrupp AG, Bayer Material Science AG, Salzgitter Mannesmann Forschung GmbH, Robert Bosch GmbH, Benteler Stahl/Rohr GmbH, Bayer Technology Services GmbH, and the state of North Rhine-Westphalia, as well as the European Union in the framework of the ERDF. Also the support from DFG under grant number STE1116/13-1 is highly acknowledged.

References

[1] W. M. R. Sekerka, Morphological stability of a particle growing by diffusion or heat flow, Journal of Aplied Physics 34 (2) (1963) 323–328.
[2] J.S. Langer, H. Müller-Krumbhaar, Theory of dendritic growth - I. Elements of stability analysis, Acta Metallurgica 26 (11) (1978) 1681–1687.
[3] J.S. Langer, H. Müller-Krumbhaar, Theory of dendritic growth - II. Instabilities in limit of vanishing surface-tension, Acta Metallurgica 26 (11) (1978) 1689–1695.
[4] J.S. Langer, H. Müller.Krumbhaar, Theory of dendritic growth - III. Effects of surface tension, Acta Metallurgica 26 (11) (1978) 1697–1708.
[5] J. Lipton, W. Kurz, R. Trivedi, Rapid dendrite growth in undercooled alloys, Acta Metallurgica 35 (4) (1987) 957–964.
[6] M. Ben Amar, E. Brener, Physical Review Letters 71 (4) (1993) 589–592.
[7] M.E. Gliksman, M.B. Koss, E.A. Winsa, Dendritic growth velocities in microgravity, Physical Review Letters 73 (4) (1994) 573–576.
[8] I. Steinbach, Pattern formation in constraint dendritic growth with solutal buoyancy, Acta Materialia 57 (9) (2009) 2640–2645.
[9] A. Badillo, D. Ceynar, C. Beckermann, Growth of equiaxed dendritic crystals settling in an undercooled melt, Part 1: Tip kinetics, Journal of Crystal Growth 309 (1) (2007) 197–215.
[10] R. Benzi, S. Succi, M. Vergasola, The lattice Boltzmann equation: theory and application, Physics Reports 222 (3) (1992) 145–197.
[11] S. Chen, G. Doolen, Lattice Boltzmann method for fluid flows, Annual Review of Fluid Mechanics 30 (1998) 329–364.
[12] F. Varnik, D. Dorner and D. Raabe, Roughness-induced flow instability: A Lattice Boltzmann study, Journal of Fluid Mechanics 573 (2007) 191–209.
[13] G. De Fabritiis, A. Mancini, D. Mansutti, S. Succi, Mesoscopic models of liquid/solid phase transitions, Int. J. Mod. Phys. C 9 (8) (1998) 1405–1415.
[14] W. Miller, S. Succi, D. Mansutti, Lattice Boltzmann model for anisotropic liquid solid transition, Physical Review Letters 86 (16) (2001) 3578–3581.
[15] W. Miller, S. Succi, Lattice Boltzmann model for anisotropic crystal growth from melt, Journal of Statistical Physics 107 (1/2) (2002) 173–186.
[16] W. Miller, Crystal growth kinetics and fluid flow, International Journal of Modern Physics B 17 (1/2) (2003) 227–230.
[17] D. Medvedev, K. Kassner, Lattice-boltzmann scheme for crystal growth in external flows, Physical Review E 72 (5) (2005) 056703.
[18] D. Medvedev, T. Fischaleck, K. Kassner, Influence of external flows on crystal growth: Numerical investigation, Physical Review E 74 (3) (2006) 031606.
[19] D. Medvedev, T. Fischaleck, K. Kassner, Influence of external flows on pattern growth, Journal of Crystal Growth 303 (1) (2007) 69–73.
[20] A. Karma, W.-J. Rappel, Phase-field method for computationally efficient modeling of solidification with arbitrary interface kinetics, Physical Review E 53 (4) (1996) R3017–R3020.
[21] A. Karma, W.-J. Rappel, Quantitative phase-field modeling of dendritic growth in two and three dimensions, Physical Review E 57 (4) (1998) 4323–4349.
[22] A. Karma, Phase-field formulation for quantitative modeling of alloy solidification, Physical Review Letters 87 (11) (2001) 115701.
[23] I. Steinbach, Phase-field models in materials science, Modelling Simul. Mater. Sci. Eng. 17 (2009) 073001.
[24] I. Steinbach, M. Appel, Multi phase field model for solid state transformation with elastic strain, Physica D 217 (2) (2006) 153–160.
[25] C. Beckermann, H.-J. Diepers, I. Steinbach, A. Karma, X. Tong, Modeling melt convection in phase-field simulations of solidification, Journal of Computational Physics 154 (2) (1999) 468–496.
[26] F. Higuera, S. Succi, and R. Benzi, Lattice gas dynamics with enhanced collisions, Europhysics Letters 9 (4) (1989) 345–350.
[27] Y. Qian, D. d'Humières, P. Lallemand, Lattice BGK models for Navier-Stokes equation, Europhysics Letters 17 (6) (1992) 479–484.
[28] X. Tong, C. Beckermann, A. Karma, Q. Li, Phase-field simulations of dendritic crystal growth in a forced flow, Physical Review E 63 (6) (2001) 061601.
[29] A. L. Kupershtokh, New method of incorporating a body force term into the lattice Boltzmann equation, in: Proc. 5th International EHD Workshop, University of Poitiers, Poitiers, France, 2004, pp. 241–246.

[30] T. Yabe, T. Aoki, A universal solver for hyperbolic equations by cubic-polynomial interpolation. I. One-dimensional solver, Computer Physics Communications 66 (2-3) (1991) 219–232.
[31] T. Yabe, T. Ishikawa, P. Wang, T. Aoki, Y. Kadota, F. Ikeda, A universal solver for hyperbolic equations by cubic-polynomial interpolation. II. Two- and three-dimensional solvers, Computer Physics Communications 66 (2-3) (1991) 233–242.